Structure and mechanical behavior of a toucan beak

Yasuaki Seki, Matthew S. Schneider, Marc A. Meyers *

Department of Mechanical and Aerospace Engineering, University of California, 9500 Gilman Drive, San Diego, La Jolla, CA 92093-0411, USA

Abstract

The toucan beak, which comprises one third of the length of the bird and yet only about 1/20th of its mass, has outstanding stiffness. The structure of a Toco toucan (*Ramphastos toco*) beak was found to be a sandwich composite with an exterior of keratin and a fibrous network of closed cells made of calcium-rich proteins. The keratin layer is comprised of superposed hexagonal scales (50 μm diameter and 1 μm thickness) glued together. Its tensile strength is about 50 MPa and Young's modulus is 1.4 GPa. Micro and nanoindentation hardness measurements corroborate these values. The keratin shell exhibits a strain-rate sensitivity with a transition from slippage of the scales due to release of the organic glue, at a low strain rate (5×10^{-5}/s) to fracture of the scales at a higher strain rate (1.5×10^{-3}/s). The closed-cell foam is comprised of fibers having a Young's modulus twice as high as the keratin shells due to their higher calcium content. The compressive response of the foam was modeled by the Gibson–Ashby constitutive equations for open and closed-cell foam. There is a synergistic effect between foam and shell evidenced by experiments and analysis establishing the separate responses of shell, foam, and foam + shell. The stability analysis developed by Karam and Gibson, assuming an idealized circular cross section, was applied to the beak. It shows that the foam stabilizes the deformation of the beak by providing an elastic foundation which increases its Brazier and buckling load under flexure loading.
© 2005 Acta Materialia Inc. Published by Elsevier Ltd. All rights reserved.

Keywords: Mechanical properties; Foams; Biological materials; Keratin; Toucan

1. Introduction

The study of biological materials can provide insights into heretofore unexploited mechanisms of designing and toughening synthetic materials [1–4]. Shells have received a great deal of attention over the past years [1,5–9] and are inspiring new processing methods for materials. The spicule of the sea urchin is another example of a biological material with mechanical properties far surpassing those of synthetic materials. It is composed of concentric layers of amorphous silica, providing a flexure strength four times higher than synthetic silica [10]. In addition, the failure is graceful and not catastrophic. Other examples, such as silk and spider web, abound. A fascinating class of biological materials is sandwich structures consisting of a solid shell and a cellular core. Karam and Gibson [11] include porcupine quills, hedgehog spines, and plant stems in this category; the cellular core increases the resistance of the shell to buckling, leading to a synergism between the two constituents.

Bird beaks usually fall into two categories: short/thick, and long/thin. The toucan is an exception. It has a long beak that is also thick, a necessity for food gathering in tall trees. This is accomplished by an ingenious solution, enabling a low density and high stiffness: a composite structure consisting of an external solid keratin shell and a cellular core. Fig. 1 shows the beak in schematic fashion. The toucan beak has a density of approximately 0.1, which enables the bird to fly while maintaining a center of mass at the line of the wings. Indeed, the beak comprises 1/3 the length of the bird, yet only makes up about 1/20 of its mass. The mesostructure and microstructure of a toucan beak reveal a

* Corresponding author. Tel.: +1 858 534 4719.
E-mail address: mameyers@mae.ucsd.edu (M.A. Meyers).
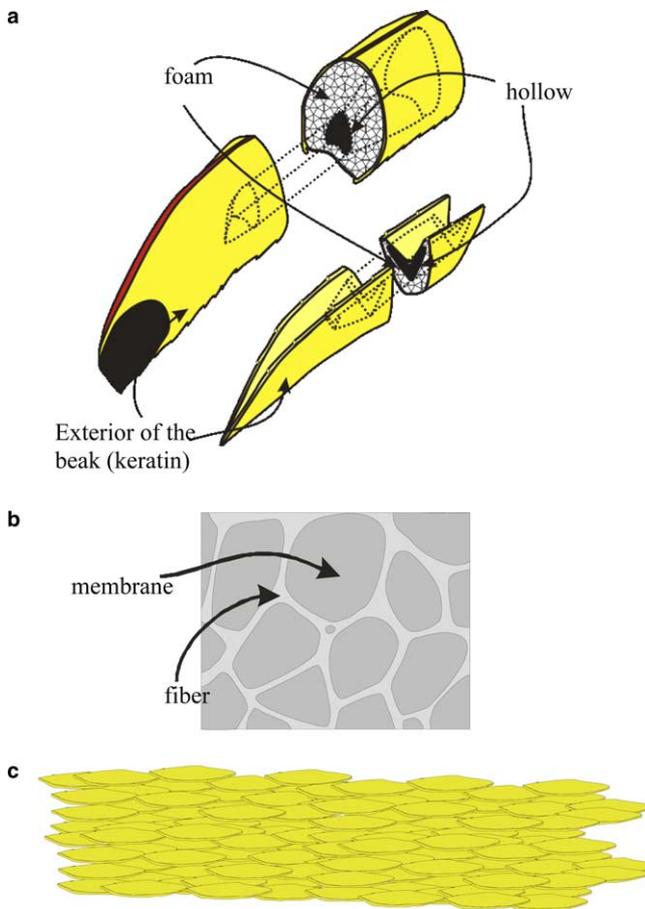
Fig. 1. Schematic representation of toucan beak: (a) overall view; (b) foam consisting of membranes in a framework of fibers and (c) keratin shell scales.

material which is reminiscent of sandwich structures of functionally graded materials, with components made of foam covered by a hard surface layer. Therefore, this biological material serves as a useful source for research and as an inspiration for structural design in engineer-

ing. This is the first study correlating the toucan beak structure to its mechanical performance.

2. Experimental techniques

The toucan beak (*Ramphastos toco*) was obtained after the natural death of animal and stored at room temperature. Both the upper beak and lower beak were used for mechanical tests and structural analysis. The black color region of the exterior beak was avoided because there is a report on the effect of starling beak coloration on hardness [12]. Humidity and temperature were measured to determine the environmental effects.

Specimen preparation for nanoindentation and microindentation was the same. The toucan beak shell was cut into small pieces by knife and mounted in epoxy. The foam was attached to a glass plate by glue. The experimental set up was the same as the one used earlier for hardness measurement of the starling beak [12]. A LECO M-400-H1 hardness testing machine with a load 100 gf was used. The indenter was applied for 15 s, and a further 45 s was allowed to elapse before the diagonals of the indentation were measured. Since nanoindentation is highly sensitive to the roughness of the sample, specimens were polished to 0.05 μm. Both the interior and exterior of beak were tested. Pictures of the samples before and after the test were taken by scanning electron microscope (SEM). A Hysistron Triboindenter was used to determine the reduced Young's modulus and hardness of the samples. Loads of 500 and 1000 μN (Berkovich-type indenter) were applied to specimens.

For tensile testing, the outer shell of the toucan beak was cut into rectangles with a knife. The rectangles were inserted into a laser cutting machine; the dog bone shape, which was programmed into the machine, had a length of 25.4 mm, width of 2.3 mm, with gage length of 6.35 mm
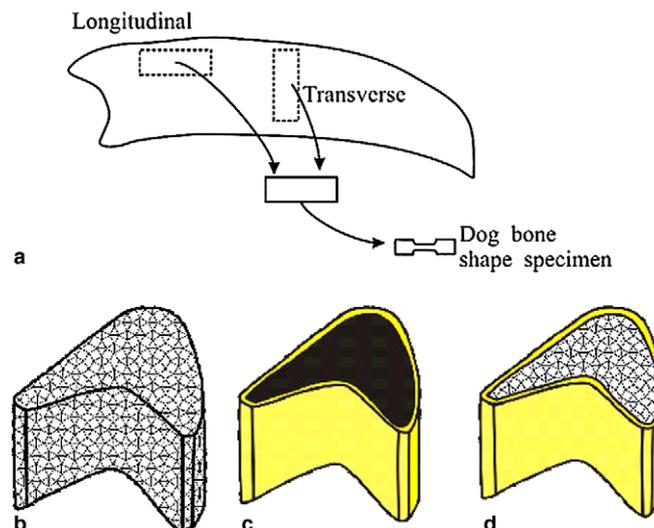
Fig. 2. Specimens for: (a) tensile testing and (b,c,d) compression testing (lower beak); (b) foam; (c) shell and (d) foam-filled shell.

and gage width of 0.5 mm. Longitudinal and transverse specimens were removed, as shown in Fig. 2(a). To avoid the effect of curvature of samples, a preload of 25 N was applied before the test. A universal testing machine equipped with a 1000 N load cell was used. Displacement was measured with an extensometer attached to the grips. The tests were carried out at room temperature and humidity of approximately 50%. The specimens for compression testing of the foam were removed entirely (as one piece) from the beak. This is shown in Fig. 2(b). The crosshead speed was 1.27 mm/min. Slices of the toucan beak were cut with a high-speed diamond saw.

The keratin exterior of the beak and foam were coated with silver nitride and placed on a Philips SEM equipped with energy dispersive X-ray analysis (EDX) for observation and characterization.

3. Results and discussion

3.1. Structure of the beak

Fig. 3(a) shows the exterior shell consisting of multiple layers of keratin scales. The thickness of each keratin scale is about 2–10 μm and the diameter is approximately 30–60 μm (Fig. 3(b)). The keratin scales are hexagonal and are attached to each other by a glue. The keratin scales are not stacked but overlap each other. The total shell thickness is approximately 0.5 mm. The SEM of Fig. 3(b) shows overlapped keratin scales that are connected by glue. The roughness of the keratin scale can be observed at a higher magnification (Fig. 3(c)).

The keratin is a protein-based fiber reinforced composite in which a high modulus fiber is embedded in a lower modulus viscoelastic matrix [13]. The matrix plays the role of a medium to transfer the applied load to the fibers, thus preventing crack propagation from local imperfections or local damaged regions [13]. Mineralization by calcium and other salts contribute to its hardness [12,14].

Most of the mechanical property studies of avian keratin are from the feathers and claws. The mean Young's modulus of feather keratin was reported to be 2.5 GPa [15]. The ostrich claw has a Young's modulus of 1.84 GPa along the length and 1.33 GPa perpendicular to it [16]. Cameron et al. [17] reported an increase in Young's modulus with distance along the *rachis* (shaft) of the feather. In contrast with this, there is little reported work on the mechanical properties of avian beak. Bonser and Witter's study [12] reports microhardnesses of 0.1 and 0.2 GPa for the yellow/light and black cycles of the European starling. The dark beak that the bird exhibits following breeding is high in melanine and twice as hard as the hardness during winter/spring. Bonser and Witter [12] proposed that the deposition of melanine granules in keratin increased its hardness.
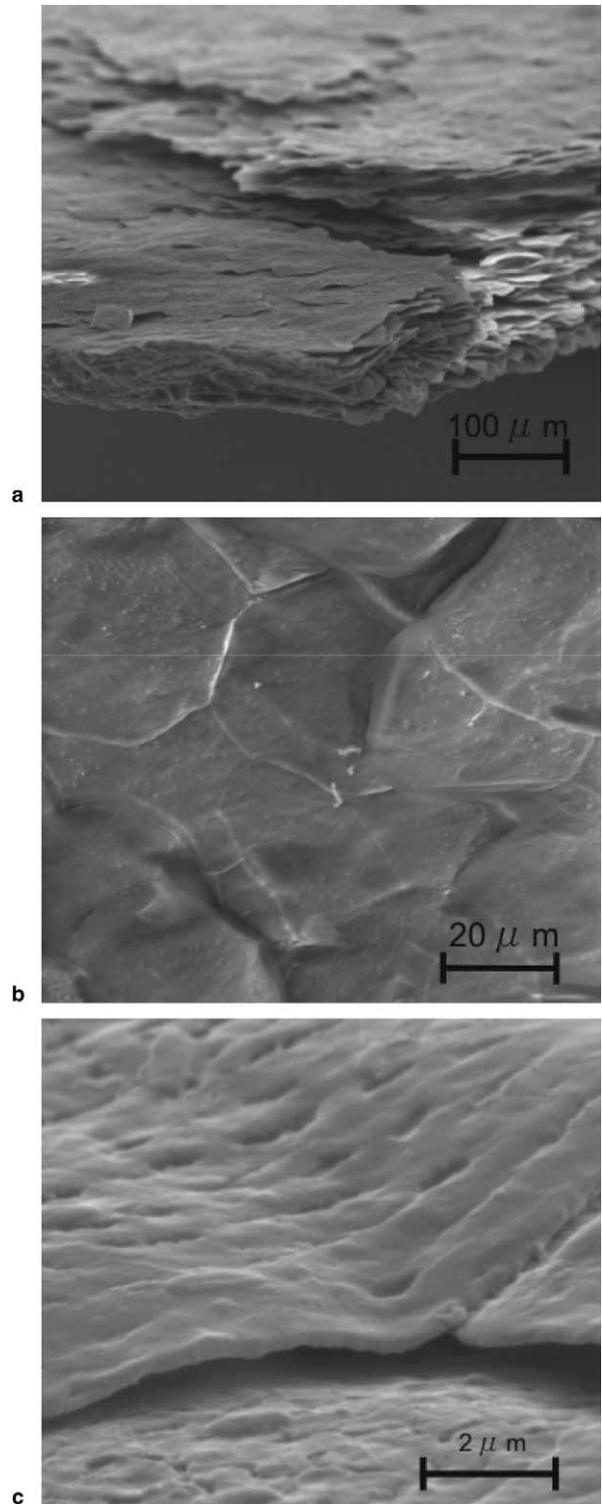
Fig. 3. Scanning electron micrograph of exterior of beak (keratin): (a) lower magnification; (b) higher magnification view of keratin scales and (c) closeup of the keratin surface.

Fig. 4 shows the inside of the beak. It is clearly a foam structure. Most of the cells in the toucan are sealed off by membranes. Thus, it can be considered as a closed-cell system. The cell sizes vary and the closed-cell
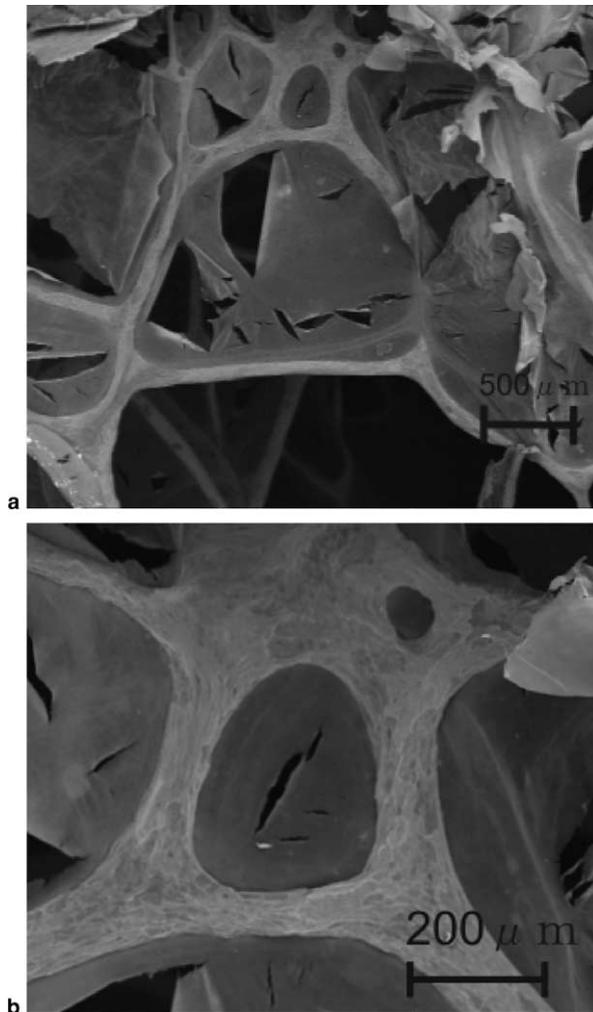
Fig. 4. Scanning electron micrograph of interior of the beak: (a) lower magnification and (b) higher magnification.

network is comprised of struts with connectivity of four, five, six or even higher.

EDX analysis (Fig. 5(a)) shows that keratin contains principally carbon and oxygen, which are the main components of the protein. A relatively low content of sulfur in the chemical component of keratin seems to point out to a low content of cystine, a sulfur-containing amino acid. The beak keratin also contains minerals as indicated by the presence of calcium (0.27%), potassium and chlorine. The presence of calcium indicates a degree of mineralization that provides the hardness of the keratin. The elements present in the membrane of the cellular core are shown in Fig. 5(b). The composition is similar to the shell keratin. Fig. 5(c) is in stark contrast with Figs. 5(a) and (b). The foam fibers contain more minerals than the membranes or the shell. No tungsten and magnesium can be seen in the membranes. Distinctively, the fibers contain 24.6% of calcium. The EDX results from fiber and membranes in the foam suggest that they are made from different materials. Membranes and fiber contained minerals, particularly the fiber was cal-

cium based protein and highly mineralized. The content of calcium is associated with the hardness of the beak keratin and fiber. The high calcium content of the fiber suggests that it is stiffer than keratin. Membranes, on the other hand, contain the same amount of calcium as the shell keratin. Hydrogen cannot be detected because it disappears during the analysis.

The EDX results can be compared with SDS analysis from several bird beaks by Frenkel et al. [18]. It is confirmed here that the Toco toucan beak keratin appears to be similar to that of other bird species, with a low sulfur and mineral content. Pautard [14] reported that the pigeon beak contains 0.28% of calcium, which agrees with our shell keratin results: 0.27–0.77%. (see Fig. 6).

3.2. Mechanical properties of the beak

3.2.1. Micro- and nanoindentation

Table 1 shows a summary of mean hardness and reduced Young's moduli of the shell keratin and fiber in the foam. The hardness of the shell keratin is 0.22 GPa from microindentation and 0.50 GPa from nanoindentation measurements. Although the same samples were tested, hardness from nanoindentation is twice as high as microindentation. The mean hardness of the fiber is 0.27 GPa from microindentation is 0.55 GPa from nanoindentation measurements. The nanoindentation results are equally higher than the microindentation ones. One of the possible reasons for the difference is the polishing of the surface, necessary for nanoindentation. However, the fibers in the foam were not polished and still exhibit higher values. There are reports of higher nanoindentation hardness than microindentation hardness for copper [19] and the same could hold true for keratin. They are explained by the pile-up effect [19]. When it occurs (as is the case with keratin and copper [19]), nanoindentation values are higher than microindentation. These differences have been discussed by Rho et al. [20,21] for bone measurements and attributed to the scale of the collagen and mineral interactions.

The loading was stopped for 5 s after the maximum was reached. Fig. 7(a) shows the constant load after the maximum; the displacement indicates an increase in the indentation depth. Viscoplastic deformation occurred for all tested keratin samples.

Fig. 7(b) shows a scanning probe micrograph of β-keratin after indentation. In indentations, two situations are possible. If the material work hardens, there will be sink-in around the indentation. If the material either work softens or has no work hardening, a pile up will be formed around the indenter. This phenomenon is well known and is described by Meyers and Chawla [22], among others. Fig. 7(b) shows clear piling-up on the surface. This result indicates that the degree of work hardening is very low and that keratin undergoes viscoplastic deformation as the load is arrested at the maximum.
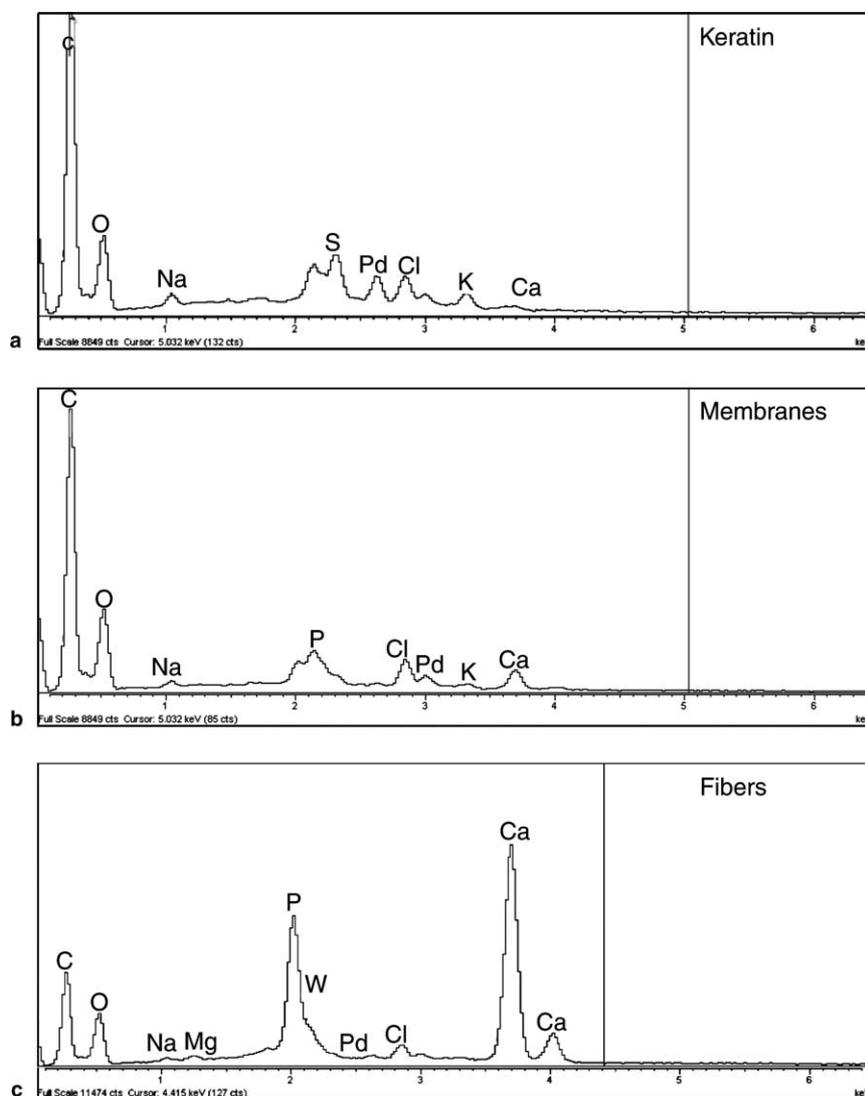
Fig. 5. Energy disperse X-ray results: (a) keratin shell; (b) foam core: membrane and (c) foam core: fiber.

3.2.2. Tensile and compressive response of beak

Typical tensile strain–stress curves of β-keratin from toucan beak, measured in longitudinal and transverse direction, are shown in Fig. 7(a). There was significant scatter in the results, which are shown in Table 2. There is no systematic difference between the Young's modulus and yield strength of keratin along the two directions. Mean values are 1.4 GPa (Young's modulus) and 30 MPa (yield strength). Thus, the keratin shell can be considered transversely isotropic.

Fig. 7(b) shows a typical compressive stress–strain curve from a lower beak specimen. Young's modulus is determined by the initial slope of the curve. The plateau region is associated with the collapse of the cell walls. After the plateau, densification of the cell wall starts. The crushing stress σ_{cr}^{*} is approximately 0.25 MPa and initial Young's modulus is approximately 30×10^{-3} GPa. Densification starts at an approximate strain of 0.9. In plateau regime, the stress does not devi-

ate significantly from 0.25 MPa. The spikes in the curve represent individual fracture events.

It is well known that the fracture of polymers is strain rate dependent. Keratin, a biological composite, also shows two different fracture modes, dependent on the strain rate. Figs. 8(a) and (b) show SEM micrographs of fracture surfaces from tensile specimens deformed at a strain rate 5×10^{-5}/s. The surface of the fracture is smooth and shows pulled out scales. Pull-out mode tends to occur in low strain rate, when large molecules can move and change their configurations during stretching. It occurs by viscoplastic shear of the inter-scale glue. Figs. 8(c) and (d) show scanning electron micrographs of fracture surfaces from tensile specimens deformed at a strain rate 1.5×10^{-3}/s. The keratin scales were completely torn and/or experienced severe visco-plastic deformation. The fracture surface can be characterized as brittle. Abundant debris from fractured scales is seen in SEM micrographs.
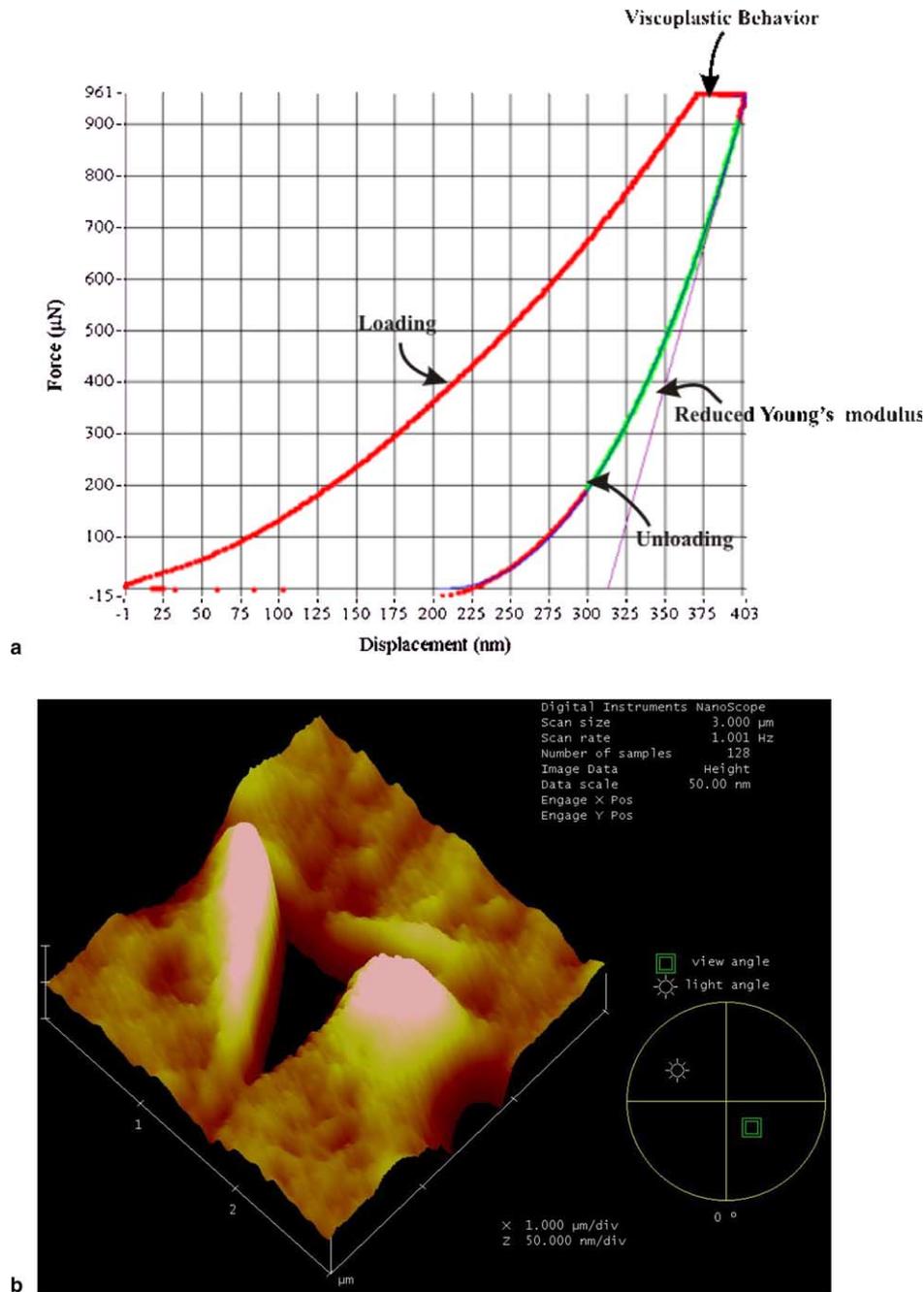
Fig. 6. (a) Force–depth for keratin using Berkovich indenter; (b) surface of keratin showing pile up around indentation.

Table 1
Summary of mean micro and nanohardness and reduced Young's modulus

	Mean hardness (GPa) microindentation	Mean hardness (GPa) nanoindentation	Reduced Young's modulus (GPa)
Shell keratin	0.22	0.50	6.7
Fiber from foam	0.27	0.55	12.7

A possible explanation for the change in failure mode is given by Fig. 9, which shows the effect of strain rate on the yield stress and the ultimate tensile strength (UTS). The yield stress is quite sensitive to strain rate, in contrast to the UTS. This can be construed as due to the viscoplastic response of the interscale glue. When the yield stress approaches (or exceeds) the UTS, fracture of the scales is preferred over viscoplastic deformation of the glue. The transition from pull out to scale fracture is governed by the criterion,

$$\sigma_t \leqslant \sigma_g \text{ or } \sigma_t \geqslant \sigma_g, \tag{1}$$
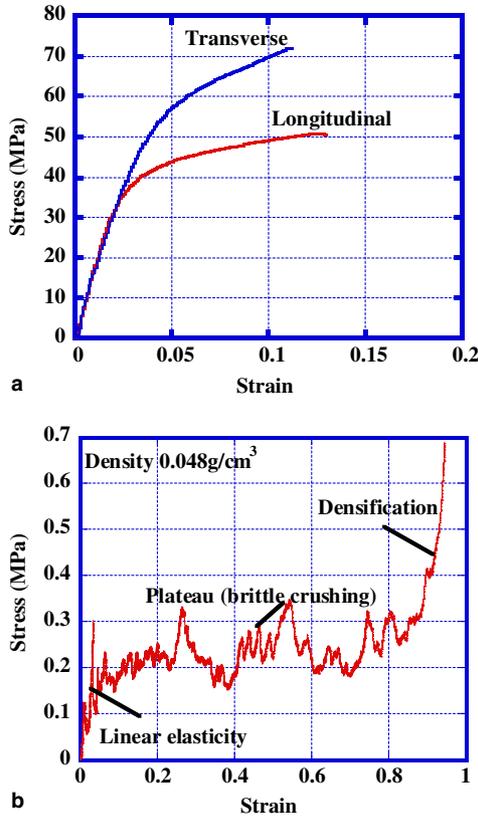
Fig. 7. (a) Tensile stress–strain curve, transverse and longitudinal directions of toucan beak shell, strain rate 8×10^{-4}/s; (b) Compressive stress–strain curve for foam.

where σ_t is the fracture stress and σ_g is the flow stress by interscale gliding. The strain rate dependence of σ_g can be expressed as

$$\sigma_g = k\dot{\varepsilon}^m, \qquad (2)$$

where m is the strain rate sensitivity. This competition between viscoplastic shear of the interscale glue and tensile fracture of the scales is similar to the response exhibited by the abalone shell in tension [9]. In the case of abalone, the tiles are made of biomineralized aragonite.

It is interesting to compare the mechanical properties of toucan beak keratin with other bird keratins from the literature. The microhardness of the toucan beak is similar to that of the European starling [12]. The Young's modulus of the toucan beak, obtained from tensile tests, is similar to the avian claw. However, it is not as stiff as feather [15,16]. The mechanical behavior of the beak appears to be very similar to avian claw keratin. The structural organization of the beak keratin is also quite similar to the avian claw and distinct from feathers [23,24]. Brush [23] determined by electrophoresis the major bands for beak keratin in a number of birds (including toucan): 16,000 and 25,000 Da (g/mole). Feathers, on the other hand, have polypeptide chains with approximately 10,000 Da [24]. Bonser [16] reported that the Young's modulus of the ostrich claw shows a 28% difference along and perpendicular to the claw directions. Toucan beak tends to be isotropic along longitudinal and transverse directions (surface of beak).

Table 2
(a) Mechanical response (tension) of keratin shell and of core foam (compression) and (b) crushing strength, density and plastic collapse strength of foam

	Strain rate(/s)	Young's modulus (GPa) (at strain 0.002)	Yield strength (MPa)	UTS (MPa)	Elongation (%)	Relative humidity %
(a)						
1 Longitudinal	5×10^{-5}	1.1	24	45	11	47
2 Longitudinal	5×10^{-4}	1.0	31	41	7	55
3 Longitudinal	5×10^{-4}	1.2	28	57	16	55
4 Longitudinal	8×10^{-3}	1.8	35	51	14	48
5 Longitudinal	1.5×10^{-3}	1.9	43	59	8	47
6 Longitudinal	1.6×10^{-3}	0.85	17	32	17	48
Average	–	1.3±0.44	29.1±9.87	47.5±10.2	12.17±4.16	–
Transverse 1	5×10^{-4}	1.9	25	40	3	47
Transverse 2	5×10^{-4}	–	–	48	8	55
Transverse 3	5×10^{-4}	1.5	31	62	10	55
Transverse 4	8×10^{-4}	1.5	45	71	11	48
Average	–	1.633±0.23	33.6±10.26	55.25±14.25	8±3.5	–
Beak average	–	1.41±0.4	30.9±9.0	50.6±11.8	10.5±4.3	–

Density (g/cm^3)	Crushing strength (MPa)	Relative density	Relative strength
(b)			
0.0309	0.065	0.0618	0.00071
0.039	0.08	0.078	0.00087
0.0497	0.225	0.0994	0.00247
0.069	0.325	0.138	0.00357
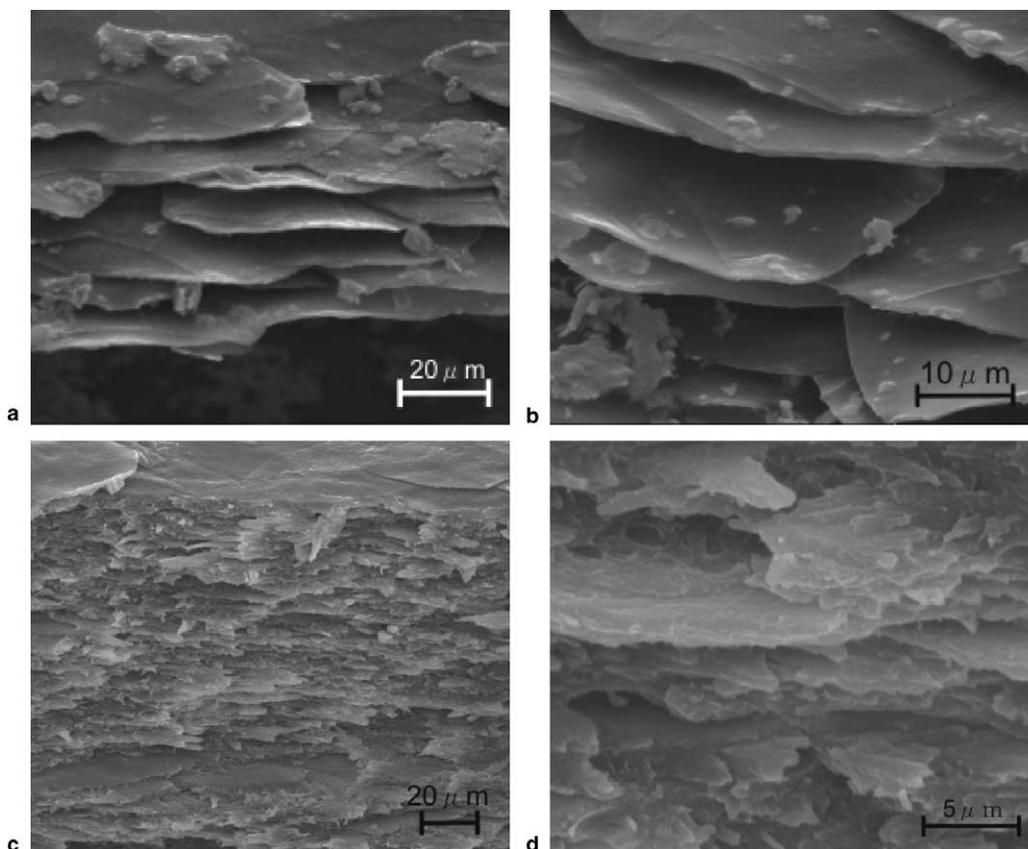
Fig. 8. Scanning electron micrographs of tensile fracture of keratin, strain rate, 5.0×10^{-5}/s: (a) lower magnification; (b) higher magnification. Scanning electron micrographs of tensile fracture of keratin, strain rate 1.5×10^{-3}/s: (c) lower magnification; (d) higher magnification.
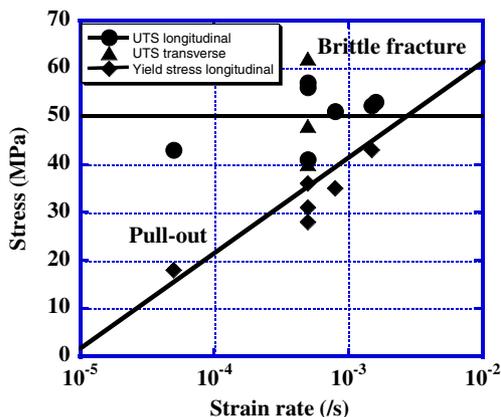
Fig. 9. Yield strength and UTS of shell keratin as a function of strain rate; notice two regimes of failure shown in figure.

Nanoindentation measurements show a higher Young's modulus and hardness than other mechanical tests. For example, Young's modulus of the keratin from nanoindentation is three times higher than the Young's modulus from tensile test data. The nanoindentation hardness is approximately two times higher than microindentation. These differences can be seen in nano-indentation measurement of bone [20,21]. Nanoindentation avoids the influences of inhomogeneities and innate

defect of the biological materials. Since nanoindentation measures only a small area of the sample, less than 1 μm range, innate defects of the material do not influence the measurement. For microindentation, the projected area is in the 100 μm range, whereas the tensile test was much bigger range so that innate defects in the biological material become significant. Nanoindentation techniques offer intrinsic mechanical properties of the material and provide useful information of the biological materials. Nanoindentation measurements provide a measure of the local mechanical properties of a material (hardness and Young's modulus). The hardness is a direct function of the material strength. Nevertheless, these values give only semi-quantitative evaluation of the mechanical performance of a material.

We observed that the failure mode changes from scale pull-out to brittle fracture as the strain rate is increased. This change can also be observed in the hoof wall [25]. The hardening behavior of keratin protects animals from natural environment. Two reasons for the variation in experimental results are innate defects in the beak and the effect of relative humidity. It is known that hydration significantly decreases stiffness and increases the ductility of keratin [26,40]. We conducted the experiments at a relative humidity varying from 47% to 55%.

For 55% relative humidity, the Young's modulus of keratin seemed slightly decreased. This effect will be systematically investigated in the future.

3.3. Analysis of mechanical response

Two aspects of deformation are addressed in this section: elastoplastic collapse of the foam, which represents the interior, and combined response of sandwich structure.

3.3.1. Modeling of interior foam (Gibson–Ashby constitutive equations)

The most significant feature of the cellular solid is the relative density, ρ^*/ρ_S (density of the cellular material, ρ^*, divided by density of the solid material, ρ_S). Gibson and Ashby [27] provide an analytical treatment for the mechanical behavior of a broad range of cellular materials. The following equation governs relative density of closed cell materials for $\rho^*/\rho_S < 0.3$:

$$\frac{\rho^*}{\rho_S} = C_1\left(\frac{t}{l}\right), \tag{3}$$

where C_1 is a numerical constant, t is uniform thickness, and l is the lateral dimension of the faces.

The toucan beak foam can be considered as a closed cell system. Deformation of the closed cells is more complicated than that of open cells. When open cell foams are deformed, cell wall bending occurs. Deformation of closed cell involves not only rotation of cell wall, but also stretching of the membranes and internal gas pressure.

The simplest closed cell cubic model was introduced to describe the deformation of the foam. Fig. 10 shows (a) undeformed and (b) deformed cubic closed cells envisaged by Gibson and Ashby [27]. The linear elastic region is limited to small strain. The foams made from material possessing a plastic yield stress are subjected to plastic collapse when load beyond the linear elastic regime. When plastic collapse occurs, there is a long horizontal plateau in the stress–strain curve. Eq. (4) represents the response of a closed-cell foam schematically represented in Fig. 10

$$\frac{\sigma_{pl}^*}{\sigma_{ys}} = C_5\left(\phi\frac{\rho^*}{\rho_S}\right)^{3/2} + (1-\phi)\frac{\rho^*}{\rho_S} + \frac{p_0 - p_{at}}{\sigma_{ys}}, \tag{4}$$

where σ_{pl}^* is the plastic collapse stress of foam, σ_{ys} is the yield stress of the solid portion, C_5 is a parameter, ϕ is the ratio of volume of face to volume of edge, p_0 is the initial fluid pressure, and p_{at} is the atmospheric pressure.

For the open cell geometry, the parameter ϕ in Eq. (4) is equal to 1. Additionally, the pressure is unchanged, i.e., $p_0 - p_{at} = 0$. Thus, Eq. (4) is reduced to

$$\frac{\sigma_{pl}^*}{\sigma_{ys}} = C_5\left(\frac{\rho^*}{\rho_S}\right)^{3/2}. \tag{5}$$

This is the open cell equation from Gibson and Ashby [27]. The parameter C_5 has an experimentally obtained value [27] of 0.3 for plastic collapse and 0.2 for brittle crushing (where $\sigma_{pl}^*/\sigma_{ys}$ in Eqs. (4) and (5) is replaced by the normalized crushing stress $\sigma_{cr}^*/\sigma_{fs}$).

The cell shape of toucan foam was characterized by measuring the mean strut connectivity at the vertex, Z_e from SEM pictures. Table 3 shows the parameters used in the characterization of the toucan foam. Euler's law for honeycombs was used to determine the mean number of struts per node, $\bar{n}$ [27]. The connectivity and number of struts per node were found to have mean values of $Z_e \approx 3.36$ and $\bar{n} \approx 4.9$, respectively. The shape of the closed cells is assumed to be hexagonal in 2-D. The mean length of struts including node thickness was estimated from 10 struts (SEM micrographs) and the parameters, t and l, measured to be 94 and 1100 μm, respectively. The Gibson–Ashby equation for a geometrical configuration of regular hexagons was applied, yielding a relative density of 0.098.
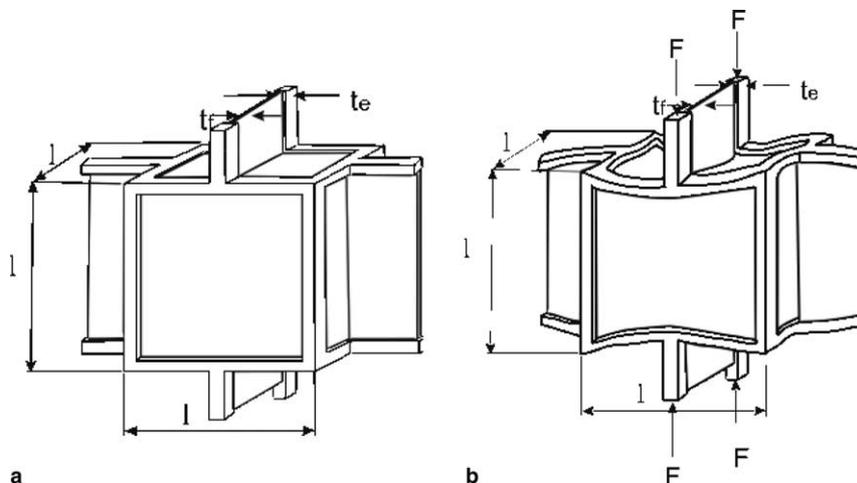
Fig. 10. (a) Gibson–Ashby model for closed-cell foam and (b) deformation of closed cell foam.

Table 3
Characterization of toucan from SEM observation

Material	Toucan foam
Density ρ^* (g/cm^3)	0.05
Open or closed	Closed
Strut connectivity Z_e	3.36
Mean edge/cell $\bar{n} = \frac{2Z_e}{Z_e - 2}$	4.94
Cell shape	Hexagon like shape in 2-D
Cell strut thickness t (μm)	94
Mean length l (μm)	1100
Relative density $\frac{\rho^*}{\rho_s} = \frac{2}{\sqrt{3}}\frac{t}{l}\left(1 - \frac{1}{2\sqrt{3}}\frac{t}{l}\right)$	0.098

There is uncertainty in the measured values of t and l due to overlapping nodes and struts. The 2-D analysis of toucan foam can be extended to the 3-D characterization from SEM observations by measuring the different cross sections of the foam. The weight of the foam was measured with an accuracy of 10^{-4} g. The parameter C_1 was found to be equal to 1.1. This is in good agreement with Gibson and Ashby's [27] estimate: $C_1 = 1$. Thus,

$$\frac{\rho^*}{\rho_S} = 1.1\left(\frac{t}{l}\right). \tag{6}$$

From Eq. (6), one can calculate the density of the fiber as approximately 0.5 g/cm^3.

The mean value of the density of the foam was measured and found to be: $\rho^* = 0.05$. Thus, the relative density of the toucan foam is approximately 0.1. The yield stress, σ_{ys}, is estimated from microindentation values ($H \approx 3\sigma_y$), which seem to be more accurate than the nanoindentation values due to the size effect. This gives a value of $\sigma_{ys} = 91$ MPa.

Fig. 11(a) shows the predictions from Eqs. (4) and (5) as well as experimental results for a number of materials [28–33]. These equations bracket the experimental results quite well. A more detailed plot of the compressive strength for the toucan foam as a function of relative density is shown in Fig. 11(b). Relative yield stress for toucan foam is less than 0.01. It is thought that the membranes tear after the animal is dead because of desiccation. Since many of the membranes contain tears, they are not expected to contribute significantly to the mechanical response of the foam. However, one would not expect this to be the case for the live animal. Gibson and Ashby [27] give values of $C_5 = 0.3$ and $C_5 = 0.2$ for plastic buckling and brittle crushing, respectively. The response of the toucan foam is intermediate between the two.

Fig. 12(a) shows the fracture pattern in the foam. It is composed of a mixture of plastic deformation, partial, and total fracture of the fibers. The fibers have a fibrous structure similar to wood and can fracture partially when they are subjected to bending (Fig. 12(b)). In other locations, the fibers undergo total fracture. Fig. 12(c) shows an example. The "green twig" appearance of the fiber is evident in Fig. 12(b). Hence, the cellular
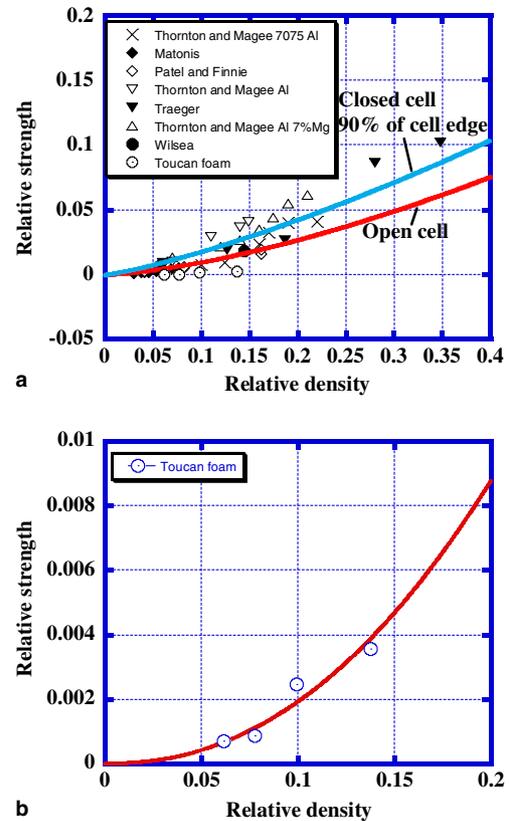
Fig. 11. (a) Experimental results (hollow circles) and Gibson–Ashby prediction for open-cell and closed cell foams (continuous lines). (b) Detailed plot.

material does not crumble when compressed to its maximum strain. Rather, it collapses in a semi-plastic manner.

3.3.2. Modeling of exterior + interior

Although sandwich structures have become commonplace in advanced systems, there are still many untapped applications. The development of synthetic foams from metals and polymers with outstanding properties like low weight, high specific stiffness and strength, reasonable energy absorption capacity, damping and insulation properties could yield novel utilizations, e.g., see [34]. One such area is in the development of crash resistant panels for the protection of vehicles. Recent reviews by Evans et al. [35,36] illustrate the importance of foams in multifunctional applications.

The objective of these tests was to establish whether the foam contributes to the strength of the beak in a measurable way. Fig. 13 shows the stress–displacement curves of the shell and foam-filled shell in compression. The geometry of the specimens is the one shown in Figs. 2(c) and (d).

After a maximum, the force levels of shell and foam-filled shell drop significantly because of buckling. The force level of the foam core increases and prevents local
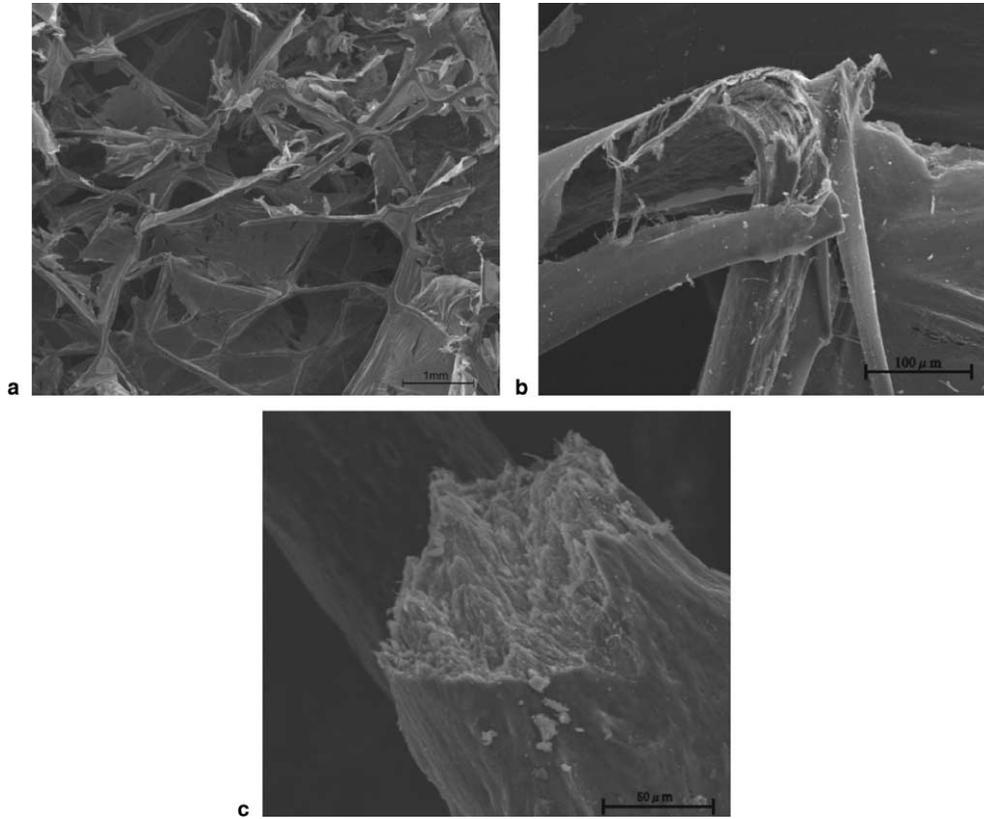
Fig. 12. Fracture morphology of closed cell foam showing profuse fiber bending; (a) overall view; (b) "green twig" fracture and (c) total fracture of fiber.

buckling. As a result, the force level of foam-filled shell is higher than the combined force of shell and foam. This effect is referred to as the interaction effect. Because of the interaction effect, the energy absorption capacity of the beak increases significantly and improves mechanical stability.

The quasistatic and dynamic mechanical response of foam-filled assemblies has been investigated by Hanssen et al. [37–39]. They used aluminum tubes with square sections filled with aluminum foam. By subjecting them to compression parallel to the tube axis, they demonstrated that there is a significant synergism between tube and foam.

A foam-filled extrusion of aluminum has been investigated by Hanssen et al. [37]. They introduced average force model described by separate average forces when square foam filled extrusion was crushed statically. The following equation describes the average force, F_{avg}:

$$F_{avg} = F_{avg}^0 + \sigma_f b_i^2 + C_{avg}\sqrt{\sigma_0 \sigma_f} b_m h, \tag{7}$$

where $F_{avg}^0 = 13.06\sigma_0 b_m^{1/3} h^{3/5}$ is the average crushing force of the non-filled extrusion, $\sigma_f b_i$ is the uniaxial resistance of the foam, $C_{avg}\sqrt{\sigma_0 \sigma_f} b_m h$ is contribution from the interaction effect between foam and extrusions. C_{avg} is dimensionless parameter. Table 4 shows the other parameters of Eq. (7).

The foam filling reduces the densification strain of the component, in comparison with non filled extrusion. The densification strain is the same as the effective crushing length, S_E. The mechanisms involved in reduction of S_E are the increased number of contacting lobes from extrusion and the densification strain of the foam. The densification of the foam can be described by following equation [27]:

$$\varepsilon_D = 1 - 1.4\left(\frac{\rho^*}{\rho_S}\right), \tag{8}$$

where ρ^* is density of the foam and ρ_S is the density of the solid.

The densification strain of foam filled extrusion, S_E, was modeled [37–39] as a force-weighted average of foam affected by densification strain of non-foam filled extrusion S_E^F and densification strain of foam ε_D

$$S_E = \frac{\left(F_{avg}^0 + C_{avg}\sqrt{\sigma_f \sigma_0} b_m h\right) S_E^F + (\sigma_f b_i^2)\varepsilon_D}{F_{avg}}. \tag{9}$$

We can estimate the average force and densification strain of the toucan beak by using the model introduced by Hanssen et al. [37–39]. The model parameters for the toucan beak and analytical data are shown in Tables 4 and 5, respectively. Fig. 13(b) shows comparison of analytical and experimental results. The predictions from
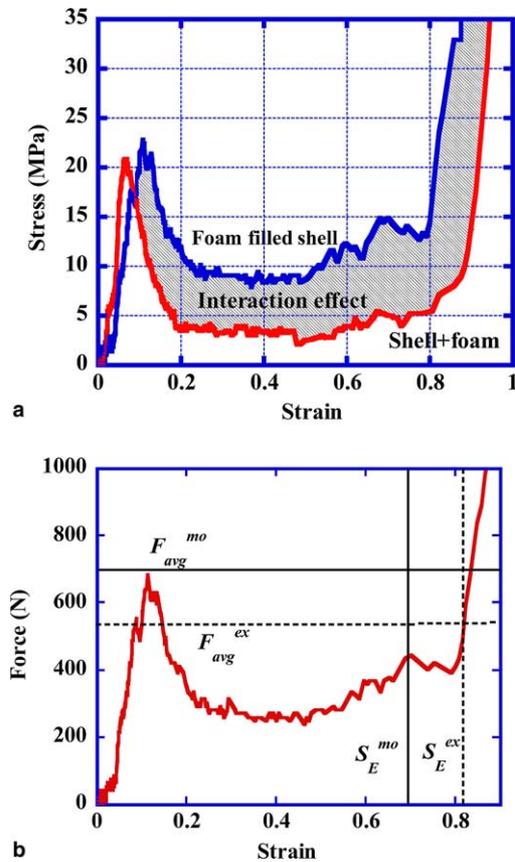
Fig. 13. (a) Compressive curves of foam, shell, foam + shell, and foam filled shell. (b) Comparison of experimental compressive response of foam-filled shell with model.

Table 5
Parameters for toucan beak (Hanssen et al. [37–39] analysis)

Model parameters	
σ_0 (MPa)	40
$\sigma_{0.2}$ (MPa)	30
σ_u (MPa)	50
σ_f (MPa)	0.2
B (mm)	23
H (mm)	0.48
b_m (mm)	22.5
b_i (mm)	22.0
C_{avg}	5
F_{avg}^{mo} (N)	683
F_{avg}^{ex} (N)	574
S_E^{mo}	0.67
S_E^{ex}	0.88

cantly increases the energy absorption in comparison with the non-foam shell.

3.3.3. Stability analysis

Karam and Gibson [41,42] and Gibson et al. [43] analyzed the elastic stability of the porcupine quill, a cylindrical shell with a foam core. The foam core acts as elastic foundation, resisting the bending of the shell. The core increases the local buckling resistance of the thin shell.

This analysis can be applied to the present case. It is interesting to note that Karam and Gibson [41] eliminated the central part of the cellular core, since they reasoned that it does not contribute significantly to the enhancement of the stability. This is exactly the configuration inside the toucan beak, as sketched in Fig. 1. The core is indeed hollow. The Karam–Gibson analysis is based on a cylindrical beam. Fig. 14(a) shows the cross section of the beak, with characteristic dimensions. We make the conversion into a cylindrical beam, shown in Fig. 14(b), with dimensions shown: diameter, $2a = 35$ mm and thickness, $\delta = 0.5$ mm, yielding $>a/\delta = 35$. This ratio is in the range given by Gibson et al. [43] for biological materials. Karam and Gibson [41] analyzed two loading configurations, shown in Figs. 14(c) and (d): compressive loading and bending.

In order to apply the Karam–Gibson equations, it is necessary to estimate the relative Young's modulus of the foam. This is accomplished through the following Gibson–Ashby [27] equations:

$$\frac{E^*}{E_S} = C_1 \left(\frac{\rho^*}{\rho_S}\right)^2. \tag{10}$$

Eq. (10) applies for open cells. The value of C_1 is approximately 1.

For closed cell foams,

$$\frac{E^*}{E_S} = \phi^2 \left(\frac{\rho^*}{\rho_S}\right)^2 + (1 - \phi)\frac{\rho^*}{\rho_S} + \frac{P_0(1 - 2v^*)}{E_S(1 - \rho^*/\rho_S)}, \tag{11}$$

the average force model F_{avg}^{mo} is higher than the experimental average force F_{avg}^{ex} and there is a 17% difference in densification strain (S_E^{mo} vs. S_E^{ex}). The cross section of the sample (lower beak) is somewhat triangular, in contrast with a square cross section used by Hanssen et al. [37–39]. The densification strain also decreases with dimension of the sample. The thickness of the shell was varied and it decreases the stiffness of the shell wall.

The calculations above demonstrate that the sandwich structure of the toucan beak is a high-energy absorption system. The presence of the foam significantly

Table 4
Model parameters for Hanssen et al. [37–39] analysis

Model parameters	
σ_0	Extrusion wall characteristic, $0.5\ (\sigma_{0.2} + \sigma_u)$
$\sigma_{0.2}$	Extrusion wall stress at 0.2% plastic strain
σ_u	Extrusion wall ultimate stress
σ_f	Foam plateau stress
B	Outer component cross section width
H	Component wall thickness
b_m	$b - h$
b_i	$b - 2h$
C_{avg}	Interaction constant of average force

Fig. 14. (a) Cross section of top and bottom portion of beak; (b) equivalent circular section for stability analysis; (c) equivalent beam subjected to compression and (d) equivalent beam subjected to bending.

where ϕ is the fraction of foam consisting of the membranes, v^* is the Poisson ratio for the foam, and P_0 is the atmospheric pressure ($= 10^{-4}$ GPa).

Karam and Gibson [41] expressed the maximum (buckling) load (in compression) and moment (in bending) in terms of the maximum values. They assumed that both foam and solid had the same Poisson ratio: 0.3. They compared equivalent beams having the same weight and outer diameter: (a) entirely concentrated in the external shell and (b) distributed between the external shell and cellular core. Hence, their calculations indicate the relative increase in load and moment bearing ability, at the same weight. For axial loading,

$$\frac{P_{\mathrm{cr}}}{(P_0)_{\mathrm{eq}}} = \frac{\left[1 + 5\frac{\lambda_{\mathrm{cr}}}{\delta}\frac{E^*}{E_{\mathrm{S}}}\frac{\rho^*}{\rho_{\mathrm{S}}}\left(1 - 2.5\frac{\lambda_{\mathrm{cr}}/\delta}{a/\delta}\right)\right]f}{0.605\left[1 + 5\frac{\lambda_{\mathrm{cr}}}{\delta}\frac{\rho^*}{\rho_{\mathrm{S}}}\left(1 - 2.5\frac{\lambda_{\mathrm{cr}}/\delta}{a/\delta}\right)\right]^2}. \tag{12}$$

For bending, two values are determined by Karam and Gibson [41]: the Brazier moment, which is the maximum value of the bending moment, and the buckling moment, corresponding the actual folding of the structure. They are given, respectively, by the following equations:

$$\frac{M_{\mathrm{Br}}}{(M_{\mathrm{Br}})_{\mathrm{eq}}} = \frac{\left[1 + 1.747\left(\frac{a}{\delta}\right)^3\frac{E^*}{E_{\mathrm{S}}}\frac{5\lambda_{\mathrm{cr}}/\delta}{a/\delta}\left(2 - \frac{5\lambda_{\mathrm{cr}}/\delta}{a/\delta}\right)\right]^{1/2}}{\left[1 + \frac{5\lambda_{\mathrm{cr}}}{\delta}\frac{\rho^*}{\rho_{\mathrm{S}}}\left(1 - \frac{5\lambda_{\mathrm{cr}}/\delta}{2a/\delta}\right)\right]^2}$$
$$\times \frac{\left\{1 + \frac{5}{4}\frac{\lambda_{\mathrm{cr}}}{\delta}\frac{E^*}{E_{\mathrm{S}}} + 0.095\frac{a}{\delta}\frac{E^*}{E_{\mathrm{S}}}\left[1 - \left(1 - \frac{5\lambda_{\mathrm{cr}}/\delta}{a/\delta}\right)^4\right]\right\}^{3/2}}{\left(1 + \frac{5}{4}\frac{E^*}{E_{\mathrm{S}}}\frac{\lambda_{\mathrm{cr}}}{\delta}\right)}. \tag{13}$$

The buckling moment, M_{1b}, is given by (Eq. 35 from Karam and Gibson [41])

$$\frac{M_{\mathrm{1b}}}{(M_{\mathrm{1b}})_{\mathrm{eq}}} = \frac{\left(1 + 1.25\frac{E^*}{E_{\mathrm{S}}}\frac{\lambda_{\mathrm{cr}}}{\delta}\right)\left(1 + \frac{0.12\frac{E^*\lambda_{\mathrm{cr}}}{E_{\mathrm{S}}\delta}}{1 + 1.25\frac{E^*\lambda_{\mathrm{cr}}}{E_{\mathrm{S}}\delta}} - \frac{3}{2}\zeta\right)(1 - 3\zeta)f}{0.312\left[1 + 5\frac{\lambda_{\mathrm{cr}}}{\delta}\frac{\rho^*}{\rho_{\mathrm{S}}}\left(1 - 2.5\frac{\lambda_{\mathrm{cr}}/\delta}{a/\delta}\right)\right]^2(1 - \zeta)}. \tag{14}$$

The parameter λ_{cr} represents a critical instability wavelength, which is equal to Eq. (7) from Karam and Gibson [41]),

$$\lambda_{\mathrm{cr}} = \frac{\delta}{[12(1 - v_{\mathrm{S}}^2)]^{1/4}}\left(\frac{a}{\delta}\right)^{1/2}. \tag{15}$$

The parameter f is equal to Eq. (9) from Karam and Gibson [41])

$$f = \frac{1}{12(1-v^2)} \frac{a/\delta}{(\lambda_{cr}/\delta)^2} + \frac{(\lambda_{cr}/\delta)^2}{a/\delta}$$
$$+ \frac{2E^*/E_S}{(3-v^*)(1+v^*)} \left(\frac{\lambda_{cr}}{\delta}\right)\left(\frac{a}{\delta}\right). \quad (16)$$

The parameter ζ represents a correction for the decrease in the moment of inertia produced by the ovalization of the circular section. It is extracted from a nomograph plot (Fig. 6 from [41]).

The toucan beak parameters can be estimated from the measurements and mechanical tests. From Fig. 14(b), we measure from actual measurements on the cross section of the upper beak: $a/\delta = 35$. The foam-free cylindrical shell has $a/\delta = 22$. We assume, to a first approximation, that $v_S = v^* = 0.3$. Inserting these values into Eq. (15), we obtain,

$$\lambda_{cr} = 1.63 \text{ mm}.$$

The ratio between the Young moduli of cellular and solid material is obtained for the closed-cell geometry (Eq. (11)). The fraction of the foam consisting of membranes is approximately equal to 0.1. This yields,

$$\frac{E^*}{E_{SF}} = 0.018.$$

However, the foam ligaments have a much higher mineralization level than the keratin shell. This is expressed in their higher Young's modulus ($E_{SF} = 12.7$ GPa, Table 2). In order to establish the ratio of the foam Young's modulus to that of the keratin shell, a correction needs to be introduced

$$\frac{E^*}{E_S} = \frac{E^*}{E_{SF}} \frac{E_{SF}}{E_S} = 0.018 \frac{12.7}{6.7} = 0.034.$$

This is almost twice the ratio for open cells. The parameter ζ is equal to approximately 0.005 for the toucan. Thus, this correction in Eq. (14) is negligible.

Figs. 15 and 16 present the Karam–Gibson predictions of the loads and moments as a function of a/δ. The range considered, from 10^0 to 10^2, represents the actual range of ratios for biological materials [43]. The results are indeed revealing. For $a/\delta = 35$, a mean value of the ratio measured for the toucan beak, the buckling load in compression is not significantly increased. Indeed, $P_0/(P_0)_{eq}$ for $E^*/E_S = 0.04$ is close to 1. However, the Brazier and buckling moments are significantly increased. The Brazier moment ratio is 8–10 and the buckling moment ratio is 2–3 for $a/\delta = 35$ and $E^*/E_S = 0.04$. Thus, the presence of a closed-cell foam increases the ability of the beak to resist bending moments signifi-
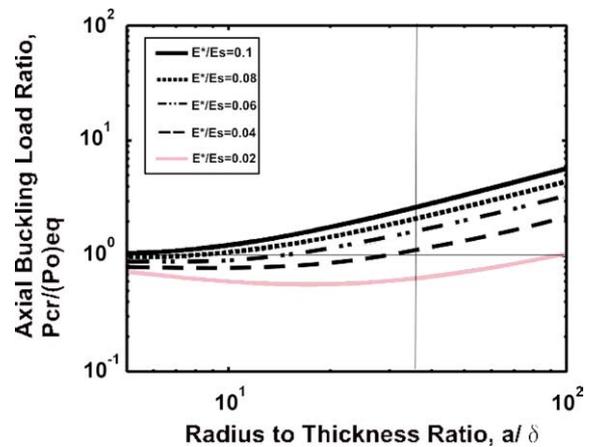
Fig. 15. Ratio of buckling load in uniaxial compression between hollow circular shell with and without cellular core, at the same weight ($\rho^*/\rho_S = 0.1$).
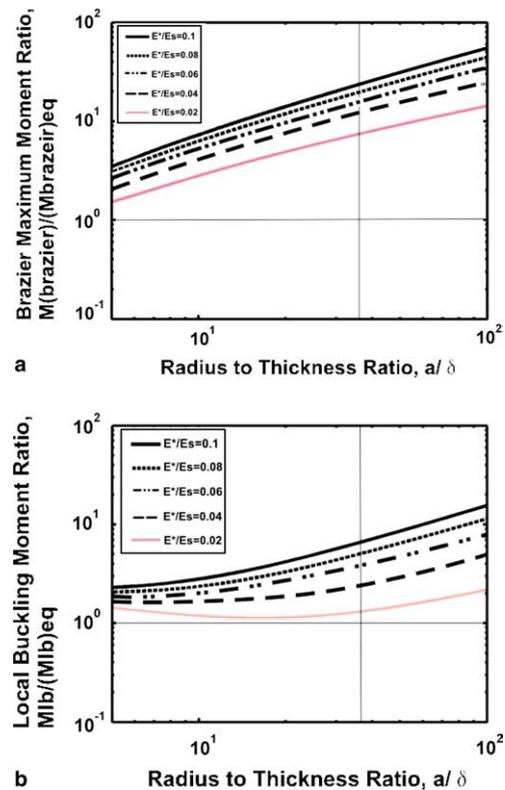
Fig. 16. Ratio of: (a) maximum (Brazier) and (b) buckling moments between hollow cylinder shell with and without cellular core, at the same weight ($\rho^*/\rho_S = 0.1$).

cantly. This is the type of loading that the beak is subjected to most commonly. It is interesting to observe that the closed cell foam presents a considerable advantage over the open-cell foam. The presence of a closed-cell foam in the beak proves that the system is indeed designed for the loads encountered by beaks.

4. Conclusion

This study of the correlation between the mechanical properties and structure of the toucan beak reveals a synergism between the external keratin shell and a cellular interior with a hollow core which optimizes the stability of the structure. The following are the principal conclusions:

- The external shell is composed of keratin scales with a diameter of approximately 50 μm and thickness of 1 μm. These keratin scales are glued together in a staggered pattern, leading to a total thickness of 0.5 mm.
- The keratin shell exhibited a failure mode that was strain-rate dependent. At 5×10^{-5}/s, failure occurred by pullout of the scales. At 1.5×10^{-3}/s, failure took place by fracture of the scales. It is proposed that the viscoplastic response of the glue is responsible for the change in failure mode.
- The foam that comprises the inside of the beak is closed cell foam. The ligaments are made of a protein rich in calcium, providing it with greater stiffness, whereas the membranes have a composition similar to the keratin shell. The toucan beak keratin has similar mechanical response and molecular structure to avian claw.
- The deformation behavior of the toucan foam in compression occurs by a mixture of brittle crushing and ductile bending ligaments. It was successfully modeled by the by Gibson–Ashby constitutive equation for closed and open cell configurations.
- The combined response of the shell and foam core was compared with the analysis proposed by Hanssen et al. [37]. The analysis reveals that there is a synergy between the shell and the foam, i.e., the energy absorbed by the shell + foam assembly is higher than the sum of the energies absorbed by shell and foam separately. We modeled interaction effect between foam and shell by using model introduced by Hanssen et al. [37].
- A stability analysis using the approach developed by Karam and Gibson [41] demonstrates that the compressive and bending buckling loads for the sandwich structure of the beak are higher than a structure of the same weight having no foam (and a correspondingly higher shell thickness).

Acknowledgements

References

[1] Sarikaya M. Microsc Res Tech 1994;27:360–75.
[2] Srinivasan AV, Haritos GK, Hedberg FL. Appl Mech Rev 1991;44:463–82.
[3] Vincent JFV. Structural biomaterials. Princeton (NJ): Princeton University Pres; 1991.
[4] Baer E, Hiltner A, Morgan RJ. Phys Today 1992;45:60–7.
[5] Mann S. Biomineralization. Oxford: Oxford University Press; 2001.
[6] Laraia JV, Heuer AH. J Am Ceram Soc 1989;72:2177–9.
[7] Menig R, Meyers MH, Meyers MA, Vecchio KS. Acta Mater 2000;48:2383–98.
[8] Menig R, Meyers MH, Meyers MA, Vecchio KS. Mater Sci Eng 2001;A297:203–11.
[9] Lin A, Meyers MA. Mater Sci and Eng 2005;390:27–418.
[10] Mayer G, Sarikaya M. Exp Mech 2002;4:395.
[11] Karam GN, Gibson LJ. Mater Sci Eng C 1994;2:113–32.
[12] Bonser RHC, Witter MS. Condor 1993;95:736–8.
[13] Fraser RD, Macrae TP. The mechanical properties of biological materials. Symp Soc Exp Biol, 34. Cambridge: Cambridge University Press; 1980. p. 211–46.
[14] Pautard FGE. Nature 1963;199:531–5.
[15] Bonser RHC, Purslow PP. J Exp Biol 1995;198:1029–33.
[16] Bonser RHC. J Mater Sci Lett 2000;19:1039–40.
[17] Cameron CJ, Wess TJ, Bonser RHC. J Struct Biol 2003; 143:118–23.
[18] Frenkel MJ, Gillespies JM. Aust J Bio Sci 1976;29:467–79.
[19] Qian L, Li M, Zhou Z, Yang H, Shi X. Surf Coat Technol 2005;195:264–71.
[20] Rho JY, Roy ME, Tsui TY, Pharr,GM. In: Transactions of the 43th annual meeting of the Orthopaedic Research Society, San Francisco (CA); 1997. p. 811.
[21] Rho JY, Liisa KS, Zioupos P. Med Eng Phys 1998;20:92–102.
[22] Meyers MA, Chawla KK. Mechanical metallurgy. NJ: Prentice Hall; 1984. p. 619.
[23] Brush AH. Biochem Syst Ecol 1986;14:547–51.
[24] Brush AH, Wyld JA. Comp Biochem Physiol 1982;73B:313–25.
[25] Kasapi MA, Gosline JM. J Exp Biol 1996;199:1133–46.
[26] Bonser RHC. J Mater Sci Lett 2002;21:1563–4.
[27] Gibson L, Ashby MF. Cellular solids: structure and properties. 2nd ed. Cambridge: Cambridge University Press; 1997.
[28] Traeger RK. J Cell Plast 1967;3:405–18.
[29] Matonis VA. Soc Plast Eng J 1964(September):1024.
[30] Thornton PH, Magee CL. Metall Trans 1975;6A:1253.
[31] Thornton PH, Magee CL. Metall Trans 1975;6A:1801.
[32] Wilsea M, Johnson KL, Ashby MF. Int J Mech Sci 1975;17:457.

[33] Patel MR, Finnie I. J Mater 1970;5:909.

[34] Band J, Dilger K. Einsatz struktureller polymer-schäume zur optimierung von automobilkarossen. In: Wielage B, Leonhardt G, editors. Verbundwerkstoffe und Werkstoffverbunde. Weinheim: Wiley-VCH; 2001. p. 507–11.

[35] Evans AG, Hutchinson JW, Fleck NA, Ashby MF, Wadley HNG. Prog Mater Sci 2001;46:309–27.

[36] Evans AG, Hutchinson JW, Ashby MF. Prog Mater Sci 1998;43:171–221.

[37] Hanssen AG, Langseth M, Hopperstadt OS. Int J Impact Eng 2000;24:347.

[38] Hanssen AG, Langseth M, Hopperstadt OS. Int J Mech Sci 2002;44:359.

[39] Reyes A, Hopperstad OS, Hanssen AG, Langseth M. Int J Impact Eng 2004;30:805.

[40] Taylor AM, Bonser RHC, Farrent JW. J Mater Sci 2004; 39:939–42.

[41] Karam GN, Gibson LJ. Int J Solids Struct 1995;32: 1259–83.

[42] Karam GN, Gibson LJ. Int J Solids Struct 1995;32: 1285–1306.

[43] Gibson LJ, Ashby MF, Karam GN, Wegst U, Shercliff HR. Proc Roy Soc 1995;450:141–62.